The X-ray Microcalorimeter Spectrometer onboard of Athena

J.W. den Herder[a], D. Bagnali[k], S. Bandler[b], M. Barbera[c], X. Barcons[d], D. Barret[e], P. Bastia[f], M. Bisotti[k]. K. Boyce[b], C. Cara[e], M. Ceballos[d], L. Corcione[g], B. Cobo[d], L. Colasanti[p], J. de Plaa[a], M. DiPirro[b], W.B. Doriese[h], Y. Ezoe[i], R. Fujimoto[j], F. Gatti[k], L. Gottardi[a], P. Guttridge[l], R. den Hartog[a], I. Hepburn[l], R. Kelley[b], K. Irwin[h], Y. Ishisaki[i], C. Kilbourne[b], P.A.J. de Korte[a], J. van der Kuur[a], S. Lotti[p], C.Macculi[p;], K. Mitsuda[n], T. Mineo[m], L. Natalucci[p], T. Ohashi[i], M. Page[l], S. Paltani[o], E Perinati[m], L. Piro[p], C. Pigot[e], F.S. Porter[b], G. Rauw[q], L. Ravera[e], E. Renotte[q], J-L. Sauvageot[e], C. Schmid[u], S. Sciortino[c], P. Shirron[b], Y. Takei[n], G. Torrioli[r] , M. Tsujimoto[n], L. Valenziano[s], D. Willingale[t], C. de Vries[a], H. van Weers[a], J. Wilms[u], N.Y. Yamasaki[n]

[a] *SRON, Netherlands Institute for Space Research, Sorbonnelaan 2, 3854 CA Utrecht*
[b] *NASA/Goddard Space Flight Center, Greenbelt, MD 20771, USA*
[c] *INAF – Osservatorio Astronomico di Palermo, Piassa de Parlamento 1, 90134 Palermo, Italy*
[d] *Instituto de Física de Cantabria (CSIC-UC), 39005. Santander (Cantabria), Spain*
[e] *IRAP, avenue du Colonel Roche 9, 31028 Toulouse Cedex 4, France*
[f] *Thales Alenia Space Italia S.p.A. S.S. Padana Superiore 290, 200900 Vimodrone, Milano, Italy*
[g] *INAF – Osservatorio Astronomico di Torino, Strada Osservatorio 20, 10025 Torino, Italy*
[h] *NIST, , Mail Stop 814. 03325 Broadway, Boulder, CO 8030, USA*
[i] *Tokyo Metropolitan University, 1-1 Minami-Osawa, Hachioji, Tokyo 192-0397, Japan*
[j] *Kanazawa University, Kakuma-machi, Kanazawa, Ishikawa 920-1192, Japan*
[k] *INFN-Physics, Department Genova University, Via Dodecameso 33, 16146 Genova, Italy*
[l] MSSL, Holmbury Street Mary Dorking, Surrey RH5 6NT, United Kingdom
[m] *INAF-IASF Palermo, Via Ugo La Malfa 153 90123 Palermo, Italy*
[n] *Institute of Space and Astronautical Science, 3-1-1 Yoshinodai, , Kanagawa 229-8510, Japan*
[o] *ISDC, University of Geneva, ch. d'Écogia 16, CH-1290 Versoix, Switzerland*
[p] *INAF/IASF-Roma, Via del Fosso del Cavaliere, 100, 00133, Roma, Italy*
[q] *CSL, Avenue du Pré-Aily, 4031 Angleur, Belgium*
[u] *ECAP, University of Erlangen-Nuremberg, Erwin-Rommel-Str. 1, 91058 Erlangen, FRG*
[r] *IFN, CNr-Roma, IFN-CNR, Via Cineto Romano 42, 00156 Roma, Italy*
[s] *INAF-IASF Bologna, via Piero Gobetti 101, 40129 Bologna, Italy*
[t] *Leicester University, University Road, Leicester LE1 7RH, UK*

ABSTRACT

One of the instruments on the Advanced Telescope for High-Energy Astrophysics (Athena) which was one of the three missions under study as one of the L-class missions of ESA, is the X-ray Microcalorimeter Spectrometer (XMS). This instrument, which will provide high-spectral resolution images, is based on X-ray micro-calorimeters with Transition Edge Sensor (TES) and absorbers that consist of metal and semi-metal layers and a multiplexed SQUID readout. The array (32 x 32 pixels) provides an energy resolution of < 3 eV. Due to the large collection area of the Athena optics, the XMS instrument must be capable of processing high counting rates, while maintaining the spectral resolution and a low deadtime. In addition, an anti-coincidence detector is required to suppress the particle-induced background. Compared to the requirements for the same instrument on IXO, the performance requirements have been relaxed to fit into the much more restricted boundary conditions of Athena.

In this paper we illustrate some of the science achievable with the instrument. We describe the results of design studies for the focal plane assembly and the cooling systems. Also, the system and its required spacecraft resources will be given.

Space Telescopes and Instrumentation 2012: Ultraviolet to Gamma Ray,
edited by Tadayuki Takahashi, Stephen S. Murray, Jan-Willem A. den Herder,
Proc. of SPIE Vol. 8443, 84432B · © 2012 SPIE · CCC code: 0277-786/12/$18 · doi: 10.1117/12.924269

Keywords: X-ray, missions, micro-calorimeter, Athena

1. SPATIAL RESOLVED SPECTROSCOPY

Spatial resolved spectroscopy in the soft X-ray band has been recognized as one of the fundamental frontiers in the development of high-energy astrophysics. Thanks to the development of arrays of microcalorimeters this field is wihin reach. Hence densities, temperatures, abundances as well as bulk and turbulent velocities can be measured for extended sources. A second feature of these sensors is that their resolution depends, in first approximation, only mildly on the energy, resulting in a resolving power of about 2000 at 6 keV which is even a major improvement compared to current grating spectrometers on XMM-Newton and Chandra.

In figure 1 we demonstrate the combination of angular resolution, spectral resolution and large area by a comparison for a 50 ks observation of the Perseus cluster. In the left side the superb angular resolution of Chandra allows for the identification of cavities and sound waves, the spectral resolution and number of counts is limited. In case of the ASTRO-H mission, to be launched in 2014, the spectral resolution is very promising but the angular resolution, combined with the limited area, limits the diagnostic capabilities to study the morphology of extended sources. The XMS instrument on Athena combines the very good spectral resolution with a good angular resolution and a sufficiently large area to exploit this capability in reasonable observation times.

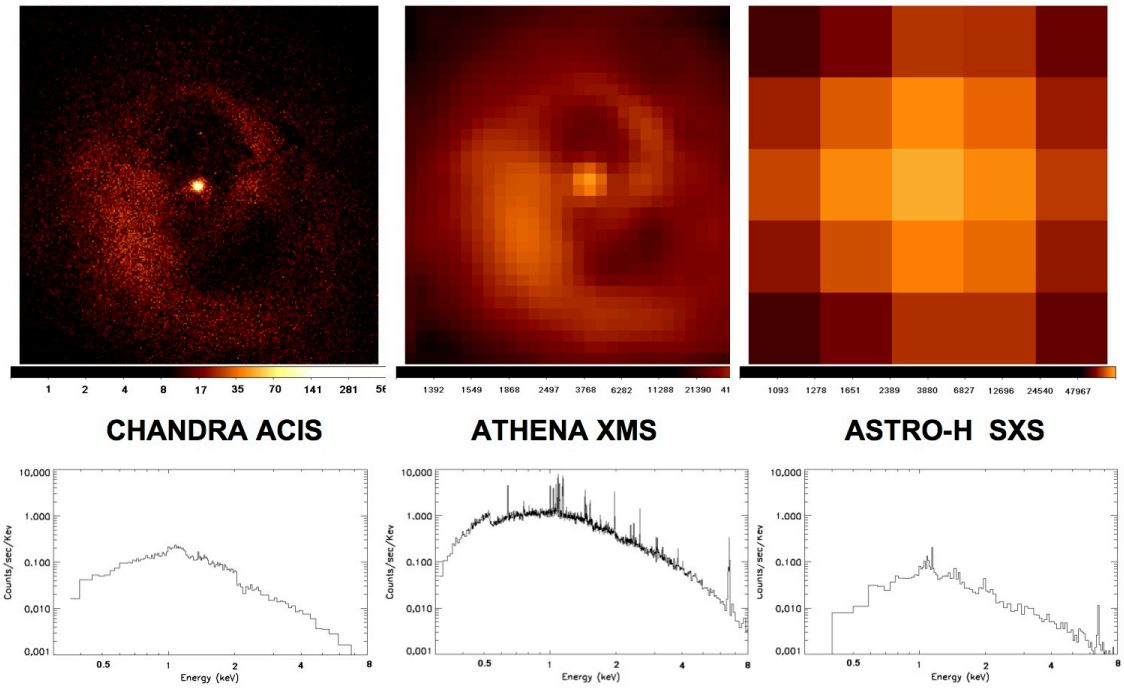

Figure 1. Comparison of the imaging capabilities for different missions for a 50 ks observation of the Perseus cluster (courtesy ESA/Dave Lumb) illustrating the strength of good spatial resolution with high spectral resolution and a sufficiently large effective area needed to fully exploit this capability in reasonable observation times.

2. INSTRUMENT REQUIREMENTS

The specific instrument requirements are derived from the top level requirements for the Athena mission [1]. Compared to the same instrument for IXO [2}, the requirements have been somewhat relaxed to reduce the programmatic uncertainty and risk (size of the array, spectral resolution). The XMS instrument will provide the capability to fully exploit the large area and high angular resolution of Athena by an imaging camera with high-spectral resolution in the focus of one of the two mirrors. Compared to ASTRO-H [3], the first mission that will fly a micro-calorimeter, the

number of pixels will increase by a factor 30, the spectral resolution by a factor 2 (requirements) and the angular resolution by a factor of 8. The key instrument requirements are listed in table 1.

Table 1: Main instrument requirements

Parameter	Requirement	Comment
Energy range	0.3 – 12 keV	Goal: 0.1 – 12 keV
Energy resolution: E < 7 keV E > 7 keV	3 eV E/ΔE = 2300	Was reduced compared to IXO where the requirement was 2.5 eV
FoV	2 arcmin	32 x 32 array with 12 m focal length equals 2.3 arcmin
Pixel size	250 μm	Demonstrated performance
good grade events	50 counts/sec/pixel	> 80% of the events will provide the 2.5 eV resolution
Absolute Time	50 μs	
Time resolution	10 μs	
Quantum efficiency @ 1 keV @ 7 keV	> 60 % > 80 %	Including filters and detector filling factor
Relative uncertainty in QE between pixel	< 3 %	Achieved by calibrations
Energy resolution uniformity (FWHM)	1 eV	Fit by a Gaussian distribution
Effective area change due to contamination over lifetime	< 10 % over 0.2 < E < 1 keV	Depending on the contaminant (water or hydrocarbons)
Non X-ray background	$2\ 10^{-2}$ counts/cm^2/keV/s	
Continuous observing time	> 20 hour	
Regeneration time	< 10%	The XMS is continuously in the focus of its optics
Energy scale stability	1 eV / h	Requires a modulated onboard calibration source

3. INSTRUMENT DESIGN

The calorimeter senses the heat pulses generated by X-ray photons when they are absorbed and thermalized. The temperature increase is proportional to the photon energy and is measured by the change in electrical resistance of the sensor. When the sensor is cooled to <100 mK and is biased in its transition between super conducting and normal resistance, a resolution of better than 2 eV has been demonstrated. The detector consists of an array of 32 x 32 absorbers which are 250 μm squared composed of 1 μm Au and 4 μm Bi to achieve the correct stopping power at 6 keV and low heat capacitance required for high energy resolution. We use a Mo/Au bilayer Transition Edge Sensor (TES) coupled to a SQUID for the read-out of the signals. For this configuration an energy resolution of <3 eV has been demonstrated. This sensor provides the 2.3 arcmin field of view and the effects of the undersampling of the mirror response (10 arcsec = 582 μm) can be quantified by using the smaller pixel sizes of the Wide-Field Imager on Athena (e.g. to identify point source contributions). For an array with 1024 TESs the thermal load by the harness still needs to be limited by using multiplexed read-out of the pixels. The Time Domain Multiplexing (TDM) scheme, where 16 pixels in the same read-out channel are sequentially sampled, is the baseline. Underneath the sensor an anti-coincidence detector is positioned to identify signals from charged particles. We have selected a segmented Si absorber (300-500 μm thick), each read-out by its own TESs. This maximizes the commonality between the electronics for the sensor and the anti-co detector. The sensor and anti-coincidence detector are segmented in 4 quadrants, reducing the effects of a potential loss in one of the read-out chains. The sensor and anti-coincidence detector signals are combined on the ground.

Whereas we will not describe in detail the performance of the detector, we will provide some background to key parameters including the spectral resolution, the count rate capability and the focal plane assembly. We end this section by a short preview on future improvements.

3.1 Spectral resolution

Spectral resolution is the key parameter for the XMS instrument. Although 3 eV has been demonstrated [7] a detailed error budget has been prepared with realistic values. This error budget is given in table 2. For typical design parameters of the sensor (T_c = 90 mK , T_{bath} = 50 mK, C = 0.8 pJ/K, n=3, α_I = 75, β_I = 1.25, R = 1 mΩ, G = 200 pW/K) the intrinsic resolution is 1.7 eV. The MUX noise allocation raises that to 2.0 eV FWHM, and the choice of record length used to extract the energy (and prerecord exclusion interval) needed to meet the count rate requirement brings the total to 2.3 eV. On top of this we include a number of contributions (at 6 keV):

- *detector non-ideal properties (excess broadening)* is an allocation for the allowable degradation for position dependence and thermalization variation in the absorber.

- *sub-mm photon noise:* The design of the blocking filters and feedthroughs must limit radiation from the next higher temperature shield that can impinge on the TES array. A limit of 0.3 eV noise from such shots corresponds to a limit on their absorbed power of 32 fW per pixel.

- *thermal crosstalk and energy input into the frame* is an allocation for the degradation from photons and cosmic rays depositing energy in the thick silicon frame of the array. This limit can be achieved by proper heat sinking of the array.

- *electrical crosstalk*: A comparable allocation is held for electrical crosstalk from inductive coupling or from non-ideal effects in the multiplexer.

- *microphonics*: The short records presumed, 2.56 ms, ensure that the first 195 Hz of signal bandwidth are lost anyway and microphonics in that range is of no consequence. The 1 eV allocation allows some microphonic contamination of the next frequency bin, such that its signal-to-noise ratio is reduced by roughly a factor of 2.

- *gain stability:* whereas long term gain variations can be calibrated, the requirement on the stability of the overall gain of the read-out electronics can be in the order of <0.0025% in 10 minutes. The non-linearity causes a 0.01% change in gain to map into a 0.012% change in assigned energy. An allocation of 0.0025% thus results in 0.12 eV FWHM of noise from gain instability.

- *ADR control:* a gain change at 6 keV of 0.115 eV/μK is expected when the non-linearity of the calibration curve is considered. This term can have a random component of 1 μK RMS as well as a drift of <4 μK over 10 minutes, for a total degradation of 0.4 eV FWHM.

- *bias noise:* the voltage noise at the top of the bias resistor (presumed to be 2.4 kΩ) is attenuated by the divider formed by that resistance and the shunt resistor. With a value of 60 nV/sqrt(Hz), which is the expected bias noise at the supply for the Astro-H/SXS calorimeter, the resulting contribution to the noise budget is only 0.1 eV, almost negligible.

- *bias stability:* Bias stability is potentially a much more significant term. A 0.01% change in detector bias causes a 0.016% change in filtered pulse height, and a 0.020% change in inferred energy. In this noise budget a less than 0.0025% bias drift in 10 minutes results in a contribution of 0.2 eV FWHM from bias instability.

- *environmental magnetic field stability:* This term is needed for the magnetic field stability and it is based on one measurement of the change in pulse height with changes in applied field near zero field.

Table 2: error budget for the spectral resolution of XMS (see also ref 11 for details)

Contribution	FWHM	units	comments
intrinsic + MUX + record size	**2.3**		For baseline detector and chosen record size to extract pulse information
detector system budget			
detector non-ideal properties	1	1 eV	excess broadening, or off design parameters
sub-mm photon noise	0.3	32 fW or 0.3 meV photons	peak of 1.3K blackbody
thermal crosstalk/frame hits	0.4	0.4 eV	
electrical crosstalk	0.4	0.4 eV	
microphonics	1	1 eV	assumes partial contamination of one freq. bin
other subsystems			
ADR control	0.4	1 uK RMS and 4 uK drift	drift over calibration time scale of ~ 10 min.
bias noise (at 2.4 kOhm bias R)	0.1	60 nV/sqrt(Hz)	is 60 fV/sqrt(Hz) at shunt resistor
bias stability	0.2	0.0025% drift in 10 minutes	N% change causes 2.0N% change in E at 6 keV
gain stability	0.12	0.0025% drift in 10 minutes	N% change causes 1.2N% change in E at 6 keV
environmental B field stability	0.4	~40 pT RMS or ~140 pT drift	based on gain vs. field measurement
margin	0.95	0.95 eV	sum of other small terms not explicitly considered
RSS of base and noise	**3.00**		

In addition to the 'static' resolution error budget slow drifts in the gain are a serious concern. With a resolution of 2000 the instrument should be very stable from observation to observation where it should be noted that the spatial and spectral load on the sensor could vary from observation to observation. In order to alleviate the requirements for the instrument stability significantly a modulated X-ray source will be part of the instrument. This source has been developed for ASTRO-H (see [4] and [5]). These sources use light sensitive photo-cathodes to generate electrons, which in turn generate the X-rays. Using LED as light source, the electrons can be pulsed (modulated) and after appropriate acceleration (11 kV) they hit a Be target coated with Cu and Cr. This results in an emission spectrum with the characteristic energies which can be used to monitor gain changes within a typical time scale of 10 minutes (assuming a 1% duty factor). The same X-rays can also be used to generate a spectrum with many more lines by fluorescence (although at a much lower intensity). This allows for an occasional calibration of the full energy scale.

3.2 Velocities

One of the key science goals for the XMS instrument is the measurement of bulk and turbulent velocities in clusters of galaxies and Supernova Remnants. The accuracy with which these can be determined does not only depend on the statistics but also on the knowledge about the shape of the redistribution function and the gain of the system. For a realistic set of simulations the effect of these gain variations from pixel to pixel and from time to time has been estimated and has a rms error of 0.6 eV (and a goal of 0.2 eV). This systematic uncertainty limits the accuracy with which bulk velocities can be measured to 32 km/s (11 km/s for the goal). This is illustrated in figure 2. The relative error between close lying emission lines is, of course, much smaller.

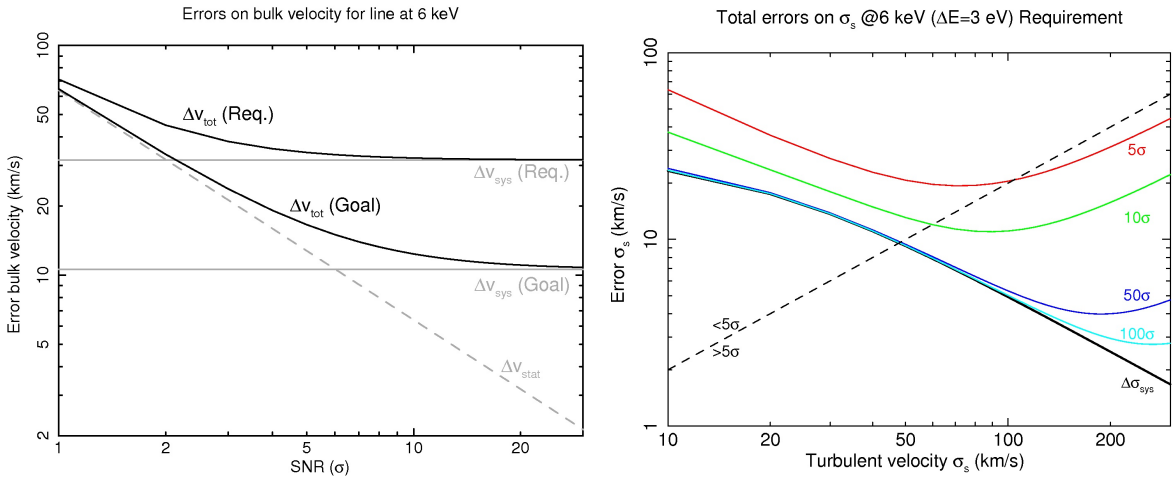

Figure 2. The error on the bulk velocity for different signal to noise ratios taking into account the uncertainty in the gain (0.6 eV). The error for the goal uncertainty in the gain (0.2 eV) is also shown (left figure solid dark lines). The statistical component and the systematic contributions are explicitly shown. In the right panel the uncertainty in the turbulent velocity is shown (see text) the dashed line denotes where the error on the turbulent velocity is 5 σ (not the line detection as such).

Also in case of turbulent velocities one needs to take into account the uncertainty in the known redistribution function. This has been calculated assuming that the same uncertainty in the gain (0.6 eV) varies on short time scales. In this case the systematic component can be calculated and combined with the statistical uncertainty. This is illustrated in figure 2 (right panel) where one can see that for a line detected by 5 σ, the error in the turbulent velocity shows a minimum of about 30 km/s at a turbulent velocity of 60 km/s.

3.3 Count rate capability

For a micro calorimeter array the fraction of events with the highest spectral resolution depends on the countrate of the incident photons (see [2]). The total number of high-resolution events for a given source, depends, of course also on the shape of the mirror PSF and the relative pointing with respect to the pixels (the PSF can be centered at a pixel, just at the corner of four pixels or anywhere in between). In our simulations we assume 10 τ and 40 τ, for the time before and after the selected event. With τ = 0.187 ms this results in a free record length of about 4.5 ms, thereby enabling 80% high-resolution events for an input countrate of 50 c/s/pixel. Using appropriate filtering the mid-res events typically have a resolution of 3.5 eV which is still very good. In figure 3 this is folded with the mirror response (FWHM of 10 arcsec) and the different event grades are shown as function of total flux on the detector and in terms of a the fraction of high-res, mid-res and low-res events and pile-up events (the time between two event triggers is less than 20 μs). As can be seen we can easily handle sources up to 0.01 Crab without noticeable degradation of the resolution and up to 0.1 Crab with small degradation of the resolution. In case of stronger sources one can insert a so-called beam diffuser in front of the detector. This is a small curved micro channel plate that diffuses the beam over a small circular ring on the detector (hence spreading the flux over more pixels). The disadvantages of this approach are that the reflectivity of the beam diffuser is less than 1 and that the reflectivity is energy dependent.

3.4 Focal plane assembly

The focal plane assembly (FPA) provides the thermal and mechanical support to the sensor and the anti-coincidence detector. In addition it accommodates the cold electronics and provides the appropriate magnetic shielding. A magnetic field attenuation of 1.6×10^5 has been achieved by two shields: a super conducting Nb shield and a cryo-perm shield at 4 K and by an appropriate cooling sequence to avoid the trapping of magnetic flux. The design, given in figure 4, is based on flight qualified components (harness and interconnections and connectors) and technology. Future development in cryo-harness and interconnections (using bump bonding) will reduce the size and mass. This has a great advantage for a cryogenic detector. The snout on top of the detector has been designed for a free field of view to the optics and includes

two optical blocking filters. The other three, needed to control the thermal load on the detector, are part of the dewar. The total mass of the focal plane assembly is 2.2 kg.

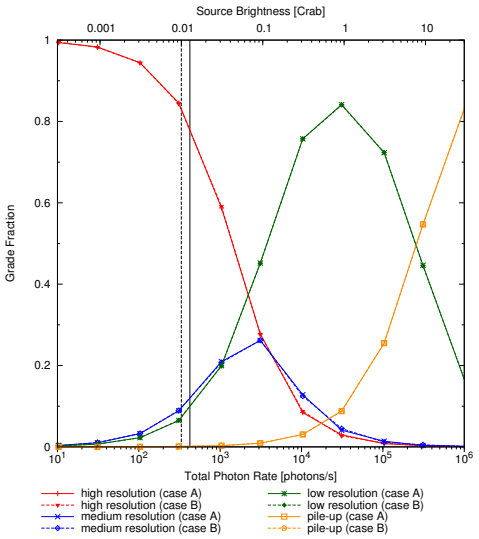

Figure 3: Count rate capability of the XMS instrument. High-resolution and mid-resolution events are identified by their relative arrival time (one needs a clean part of the data to perform proper pulse fitting). The two vertical lines denote the 50 counts/sec/pixel requirement. The two lines show the difference for the two extreme conditions with the PSF centered at a pixel or just between 4 pixels. Low-resolution events and pile-up events (arrival time within 20 μs) are also shown.

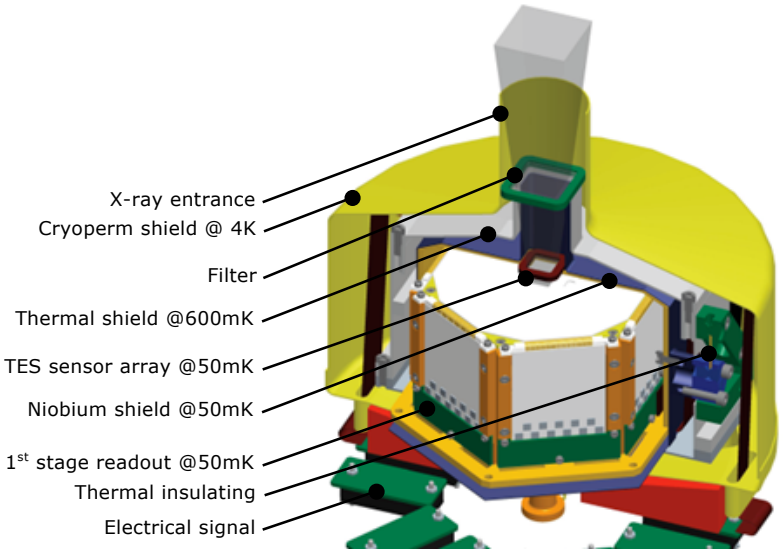

Figure 4. 3D design drawing of the focal plane assembly. The outer shield is at 4 K. Between the detector, which is at 50 mK and the outer shield there is an intermediate radiation shield at 0.3 to 0.6 K (gray). The temperature stage is also used to thermally anchor the wiring. The electronics (SQUIDs, filters etc) is mounted on the side walls of the focal plane assembly to enable a compact design (white surfaces).

3.5 Future performance

Following the decision of ESA to select Juice as first L-class mission there is additional time to improve the performance of the XMS instrument and to advance its technological and programmatic readiness. Some key areas that are being explored include:

- Increasing the number of pixels per channel allows the increase of the field of view with no immediate penalty on resources (mass, power and budget). In the current design we have assumed 16 pixels per channel but 24 or even 32 are well feasible. By further improvement in TDM performance the margin for the detector error budget and the engineering margin will improve. In the past year work has progressed in different ways to improve MUX performance. In principle, the TDM MUXed performance can improve: high sampling rate (factor 4), flux-actuated switches (factor between √2 and 2) and SQUID noise and linearization improvement (factor √2).

- A change from Time Domain Multiplexing to Code Division Multiplexing [9] allows for the increase in number of pixels multiplexed. In the figure 5 we show results from an 8-pixel CDM demonstration. The seven modulated pixels are all sub-3 eV. As is usual in CDM, pixel 0 is not switched like the other pixels, and so it has degraded resolution due to worse 1/f and pickup. We only show it for completeness. Just as for the recent TDM measurements, the frame rate is t_row = 400 ns. The 400 ns frame rate used for these measurements was somewhat conservative and not yet optimized.

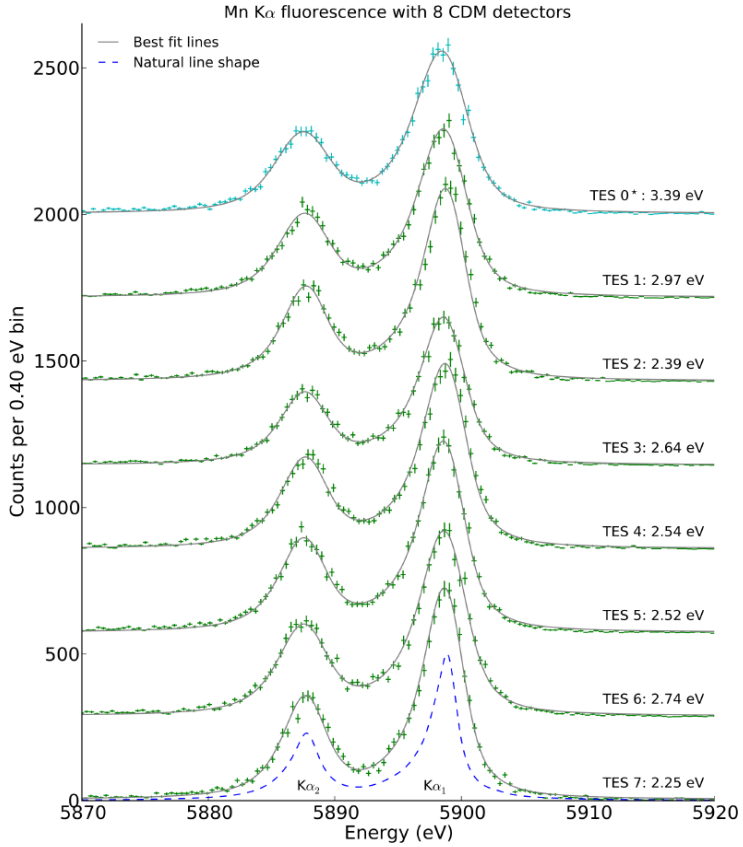

Figure 5. The MnKα spectra from an 8-pixel CDM experiment using flux-couple coded division multiplexing with a resolution better than 3 eV (except for channel 0), Data previously published by Stiehl, et al. [9]

- Finally, a change from Time Domain Multiplexing to Frequency Domain Multiplexing can be considered. Whereas the spectral resolution has so far been lagging behind (a demonstrated resolution of about 4 eV, see figure 6 right panel) it is expected that this can be improved by optimizing the magnetic shielding of the detector. For Spica/Safari, it has been demonstrated that multiplexing up to 57 channels meets the noise specification (figure 6 left panel) and a major advantage in case of a European realization of this instrument is that we can fully exploit the heritage of the development for Spica/Safari (which in turn used the developments for an X-ray calorimeter as starting point).

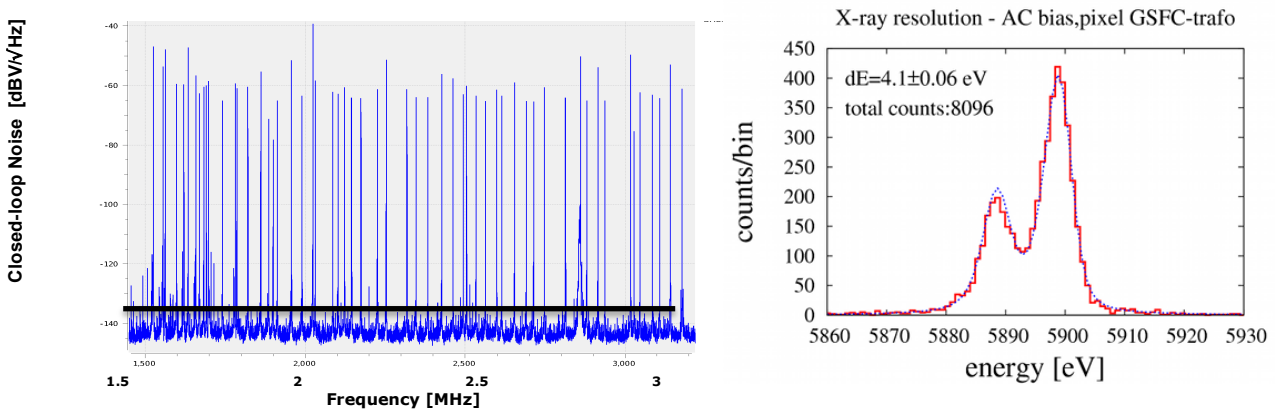

Figure 6. Left: closed-loop noise measurements for Frequency Domain Multiplexing obtained at the DAC generating the feedback signal, when 57 loops were closed at a bath temperature of 120 mK and carriers switched on (right). The horizontal lines indicate the noise level equivalent to 10 pA/√Hz at the input of the SQUID, which is the requirement for Safari and Athena. Right: optimal resolution on an AC-biased pixel (GSFC pixel design) showing the current state of the art.

4. COOLING CHAIN

The cooling chain is split into two major components: the last stage cooler which cools to 50 mK from a temperature that is between 2 and 4 K and the rest of the cooling chain that provides the cooling power to this 2 - 4 K stage. The last stage cooler can be cycled at regular intervals, allowing for regeneration, whereas the cooling chain from room temperature has to provide continuous cooling. The full cooling chain, originally designed for IXO [2] has been updated. For ease of reference we include in figure 7 the schematics of the cooling chain. It includes a 3 stage ADR for the last stage, 2 JT coolers providing the 4K base temperature for the ADR (pre-cooled by three 2-stage Stirling coolers) and two 2-stage Sitrling coolers to cool the internal shields. One shield can be cooled by LN2, allowing for faster cool down during ground testing. This configuration allows for the failure of any of the mechanical coolers as, under nominal conditions, the coolers run typically at 50% of their capacity and even with a single failure there is a safety margin (at least 15% or better in case of a failure).

By the location of the three salt pills in a triangular configuration with an outer diameter of 20 cm and a maximum length of 28 cm, and allowing the JT cold heads to intrude in this volume where the salt pill is relatively short and in between the two other salt pills, it is possible to minimize the size of the dewar. In the current design we still have reasonable margins. For this design we have calculated the hold times. The 1st stage is designed with mass of 400 grams of chrome potassium alum (CPA) whereas for the 2nd and 3rd stage the ASTRO-H design and dimensions are used. The total heat load (at 45 mK) will be 2 μW plus an estimated 0.25 μW of parasitics. This yields a hold time prediction of 24 hours and a temperature stability of < 0.4 μK rms (with a 10 Hz temperature measurement band width) at the lowest detector base temperature and typically < 0.1 mK rms at the two other temperatures. This is well within the requirements. The typical cycling of the ADR is shown in figure 9.

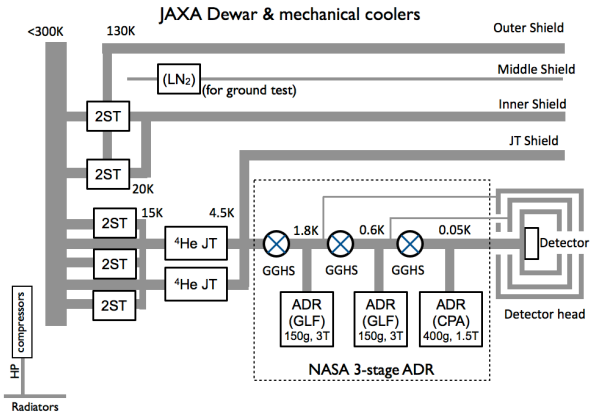

Figure 7. Schematics of the 3 stage ADR selected as baseline for the XMS last stage cooler from 4 K to 50 mK

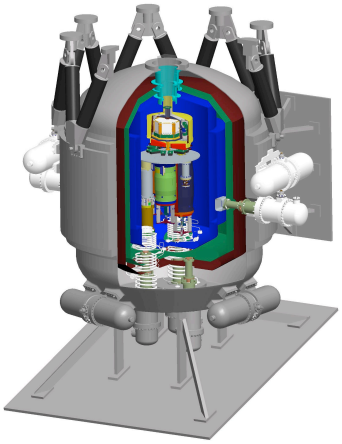

Figure 8. Realistic drawing of the XMS cooler

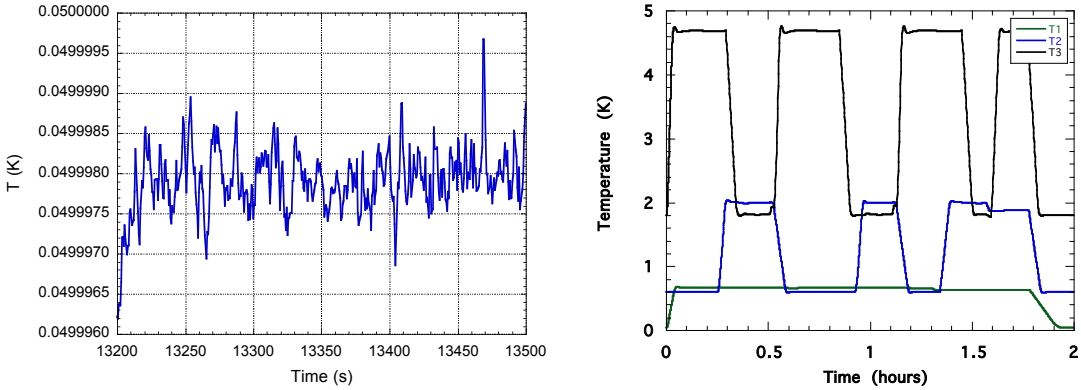

Figure 9. Simulated stability of < 0.4 μK rms for the 50 mK level (left) and switching of the three ADR staged during the regeneration (right).

Alternatively the last stage cooling chain (from 4 K to 50 mK) can also be replaced by a sorption/ADR combination which is under development for the Safari instrument on SPICA (see ref 10). This requires a different optimization of the design of the full cooling chain but no show stoppers have been identified. Detailed modeling has not been completed for this design but it was considered as the baseline for programmatic reasons.

The mass of the dewar and cryocoolers is about 201 kg, the drive electronics slightly less than 60 kg and the required electrical power is about 540 W.

5. SYSTEM DESIGN

The system design is shown in figure 10. The front end electronics (FEE) read-out the detector and is placed in close proximity of the dewar. As the detector is sensitive to EMC, a dedicated and properly filtered power supply unit (PSU) is used. The SQUID multiplexer control, the data digitization and the generation of the feedback signals take place in the digital electronic box (DE). This functionality is combined with that of the event processing functionality (EP). The EP includes two major functions: event triggering and pulse height analysis. For practical reasons the DE/EP functionality is split over two separate units. The handling of the anti-coincidence detector is completely separated from the main event chain. The number of charged particles is sufficiently small that correlation with the detector can be done on ground (the event processing functionality will reject events where multiple pixels are triggered in the detector proper). The

instrument control unit (ICU) and power distribution unit (PDU) are cold redundant and interface with the satellite. The total mass for the electronic units is 62 kg and 280 W. Some relevant key features of the design include:

- For redundancy the whole signal chain is split in 4 independent quadrants. If there is a failure in one of those, the 3 other quadrants will not be affected.
- Unregulated power is supplied to most units as they require relatively high power levels, only for the FEE (well filtered) and for the FWE/FWA this is not the case as the power levels for this later unit is very small
- The ICU is cold redundant
- The interfaces between the units (not the unit and the cryostat) are Spacewire except where there is a high volume of data (in which case optimized interfaces are used)
- Some functions as opening valves will be under control of the satellite

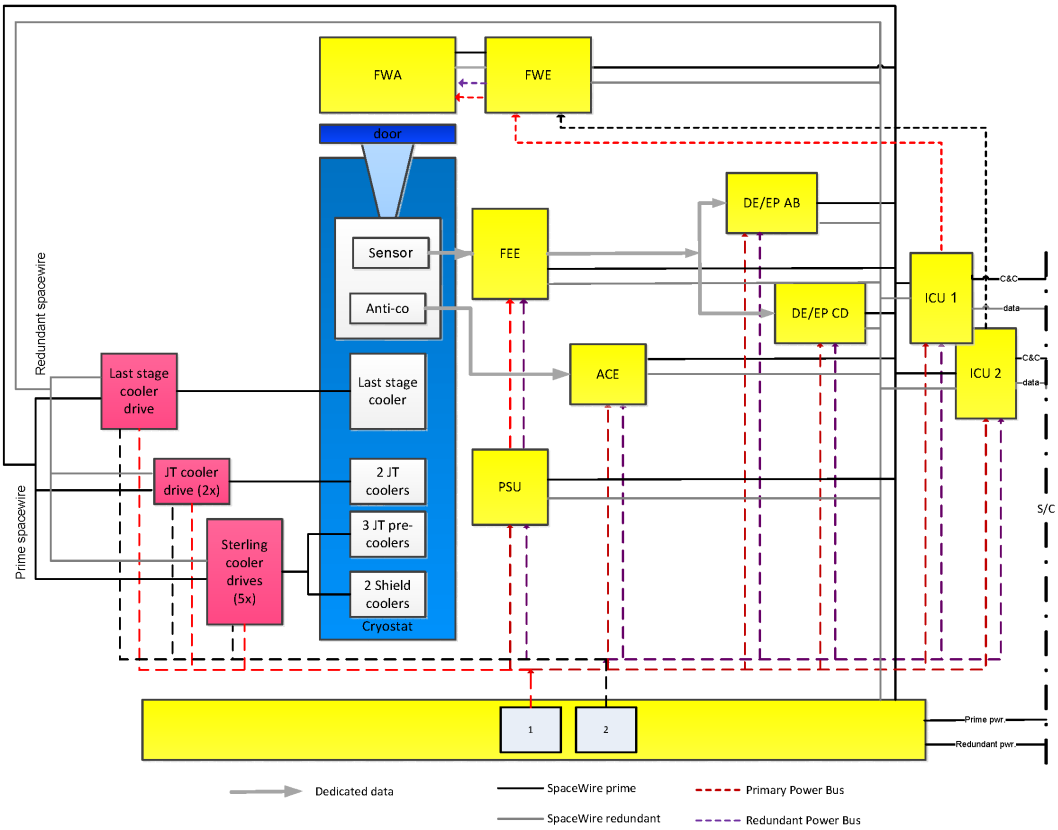

Figure 10. The X-ray Micro-calorimeter Spectrometer system design (prime and redundant power are shown (dashed, different colors for prime and redundant) as well as the Spacewire interfaces (solid lines, gray and black for prime and redundant)). Each ICU can control the units through either the prime or redundant Spacewire interface (Spacewire router). For detector data (sensor and anti-coincidence detector) a dedicated interface will be used.

In addition a filter wheel unit (FWA) can insert filters in the beam. This unit is controlled by an electronics box (FWE) as this allows for redundancy with both instrument control units. This filter wheel includes filters to reduce the optical load on the detector for the observation of bright stars, a beam diffuser for observation of very bright (point) sources and a closed position to protect the detector against micro-meteorites. For the closed position a thick Be filter is selected. This allows to optimize the number of high-resolution events at energies > 3 keV at the expense of suppressing the low energy part of the spectrum. The Filter Wheel Assembly (FWA) will also include the modulated X-ray sources, needed to correct for slow (> 10 min) gain drifts in the detector. Between the focal plane assembly and the ambient environment of the dewar a set of 3 optical blocking filters is required to reduce the thermal load on the detector to reasonable levels.

Of course, the cooling chain needs its dedicated drive electronics for the last stage cooler, the shield coolers (two 2-stage Stirling Coolers) and the two ^{4}He JT coolers with the three 2-stage Stirling pre-coolers.

The total mass of the instrument, including a 20% margin, is 409 kg and it requires about 1 kW of power (including a 10% margin). The cool down of the instrument will take about 4 weeks and during operation the regeneration time is < 2 hours whereas the hold time is about 24 hours. The expected telemetry rate is 64 kbit/s (typical) with a maximum of 840 kbit/s (bright sources).

6. CONCLUSIONS

In this paper we have presented the design of the X-ray Micro-calorimeter Spectrometer onboard of Athena. Based upon conservative selection of technology it is possible to meet the instrument requirements within the given mass, power and volume of the model payload. Considering the potential launch date of a new X-ray observatory, we expect to be able to reduce the programmatic risks by the realization of a demonstrator and also to improve the performance. By increasing the number of multiplexed pixels per read-out channel from 16 to 24 or even 32, one can increase the GRASP by a factor 2 or 4 without the need for additional spacecraft resources (mass, power, volume).

7. ACKNOWLEDGEMENT

The authors wish to acknowledge the valuable contributions from the ESA study team (D. Lumb, D. Martin, N. Rando and their colleagues). In addition we have made gratefully use of the information provided in the ESA yellow book that was written by a large team of scientists led by Xavier Barcons.

REFERENCES

[1] *Athena, the extremes of the Universe: from black holes to large-scale structures*, ESA/SRE(211)17
[2] den Herder, J.W. et al, The x-ray microcalorimeter spectrometer onboard of IXO, Space Telescopes and Instrumentation 2010: Ultraviolet to Gamma Ray. Eds. Arnaud, M., Murray, S.S., Takahashi, T. SPIE, Volume 7732, pp. 77321H-77321H-10, 2010
[3] Mitsuda, K., et al., "The high-resolution x-ray microcalorimeter spectrometer system for the SXS on ASTRO-H", Space Telescopes and Instrumentation 2010: Ultraviolet to Gamma Ray. Eds. Arnaud, M., Murray, S.S., Takahashi, T., SPIE, Volume 7732, pp. 773211-773211-10, 2010
[4] Gendreau K.D, et al., a modulated X-ray source for in-flight calibration of high-energy astrophysics instrumentation, SPIE Volume 8443-98, 2012
[5] De Vries, C.P. et al., Calibration sources for the soft x-ray spectrometer instrument on ASTRO-H, SPIE 8443,-188, 2012
[6] Shirron P. et al, "Design of a 3-stage ADR for the soft X-ray spectrometer instrument on the Astro-H mission" Proc SPIE 7732-37
[7] Kilbourne, C. et al., "Multiplexed read-out of uniform arrays of TES X-ray microcalorimeters suitable for Constellation-X ", Proc SPIE 7011, 701114
[8] R. den Hartog *et al*., *IEEE Trans. Appl. Supercond.* **21**, No. 3, Part 1, 289 (2011)
[9] G.M. Stiehl et al., "Code-division multiplexing for x-ray microcalorimeters", Appl. Phys. Lett. 100, 072601 (2012)
[10] Roelfsema, P.R. et al., The Safari imaging spectromet3r for the SPICA space observatory, Proc. SPIE 8442-24
[11] W.B. Doriese, et al., JLTP 167, 5-6, pp595-601 (2012), (DOI 10.1007/s10909-012-0509-7)